Atmospheric
Chemistry
and Physics

Measurement report: Aerosol and cloud nuclei properties along the Central and Northern Great Barrier Reef – impact of continental emissions

E. Johanna Horchler[1,a], Joel Alroe[1], Luke Harrison[2], Luke Cravigan[1], Daniel P. Harrison[2,3], and Zoran D. Ristovski[1]

[1]International Laboratory for Air Health and Quality, Queensland University of Technology, Brisbane, 4001, Australia
[2]National Marine Science Centre, Southern Cross University, Coffs Harbour, 2450, Australia
[3]School of Geosciences, University of Sydney, Sydney, 2006, Australia
[a]now at: Department of Chemistry, Faculty of Natural Science, Aarhus University, Aarhus C, 8000, Denmark

Correspondence: E. Johanna Horchler (eva.horchler@qut.edu.au)

Abstract. The frequency of coral bleaching events increased during the past decade in the Great Barrier Reef (GBR) due to climate change, and rising ocean temperatures. Recent work has demonstrated that enhancing local-scale cloud albedo can reduce the sea surface temperatures (SSTs) in this region. However, little research has been done on variations in the aerosol properties, as well as aerosol–radiation and aerosol–cloud interactions over different regions of the GBR, which is critical for predicting the potential for marine cloud brightening (MCB) climate forcing on a local or regional scale. Here, we examined trends in the aerosol population in terms of their physical and cloud condensation nuclei (CCN) properties during a research cruise in the Central and Northern GBR. Overall higher particle number concentrations, CCN number concentrations, and CCN activation ratios were observed during periods where the air masses passed over the continent prior to reaching the research vessel, despite lower hygroscopicity parameters. We suggest that organics contribute considerably to CCN number concentrations in this region of the GBR, which highlight the important role of additional emissions from inland Queensland. As well as the total aerosol number concentration, precipitation history along the back trajectory affected CCN number concentrations. These results represent a first step towards building a climatological understanding of aerosol and CCN properties over the GBR during summertime, a region and season where no observations have been previously reported.

1 Introduction

The Great Barrier Reef (GBR) covers an area of $344\,000\,\text{km}^2$ and stretches over $2300\,\text{km}$ in latitude along Eastern Australia's coastline. It is the world's biggest living structure, and home to over 600 coral varieties (Mallet et al., 2016; Hock et al., 2019; Condie et al., 2021).

Thermal stress disrupts the symbiotic relationship between corals and some algae species, causing coral bleaching (Berkelmans et al., 2004; Hughes et al., 2017). Higher levels of coral mortality are typically the result of prolonged

and severe coral bleaching (Hughes et al., 2017). In addition, the frequency of bleaching events has increased because of climate change, and rising ocean temperatures (Hughes et al., 2017; Hock et al., 2019; Stuart-Smith et al., 2018; Condie et al., 2021), with four out of the six mass bleaching events over the GBR occurring in the past 7 years (1998, 2002, 2016, 2017, 2020, and 2022) (Hughes et al., 2017; Condie et al., 2021; GBRMP, 2023). Under future climate change scenarios, this phenomenon is likely to intensify and become more frequent (Berkelmans et al., 2004). Even though reduction in greenhouse gas emissions have been attempted and

climate interventions have been implemented in recent years to mitigate the effects of climate change on the GBR, emission reductions are no longer sufficient to ensure the survival of the GBR as we know it. A loss of 4.4 % of total coral cover is observed on average every decade, with an increase in the loss rate predicted in the next few decades (Condie et al., 2021).

Local-scale cloud cover has been demonstrated to affect sea surface temperatures (SSTs) on the GBR and appears to be important in mitigating or exacerbating coral bleaching through its effect on the ocean heat budget (Leahy et al., 2013; Zhao et al., 2021, 2022). Knowledge on the aerosol number concentration, chemical composition, and size, as well as aerosol–cloud interactions over the GBR is required to estimate aerosol effects on radiation reaching and leaving the sea surface. Aerosol–cloud interactions refer to the aerosol's ability to act as cloud condensation nuclei (CCN) influencing cloud microphysical properties (Murphy et al., 1998; Andreae and Rosenfeld, 2008; Zhao et al., 2024). Modelling these effects is difficult due to the variations in numerous input parameters, as well as the complexity of the interdependent processes involved (Andreae and Rosenfeld, 2008; Cropp et al., 2018; Cravigan et al., 2020; Fiddes et al., 2021), and measurements of such over the GBR. As a result, aerosol–cloud interactions constitute by far the biggest contributor to overall uncertainty in radiative forcing modelling (Masson-Delmotte et al., 2021).

Aerosols over the marine environment can be locally derived or transported from elsewhere. Marine sources of aerosols and therefore CCN are mainly from sea spray or from secondary marine sources. Sea spray aerosol (SSA) is formed through bubble bursting, and is primarily composed of sodium chloride, other inorganic salts, and some organic compounds produced by marine biota (Heintzenberg et al., 2000; Cravigan et al., 2020). Secondary marine aerosols (SMAs), a mixture of non-sea salt (nss) sulfates and organic compounds are generated from the oxidation of aerosol precursors (Quinn et al., 2017; Jackson et al., 2018). In addition, land outflows carrying terrestrial emissions might change aerosol composition and loading over the GBR. In addition, precipitation and particle entrainment from the free troposphere (FT) have been previously found to alter the particle size distributions and CCN number concentration in marine environments (Tunved et al., 2004; Andreae and Rosenfeld, 2008; Quinn and Bates, 2011; Clarke et al., 2013; Atwood et al., 2017; Khadir et al., 2023).

The Reef Restoration and Adaptation Program (RRAP) is a collaboration of Australia's leading experts to create a suite of innovative and targeted measures to help preserve and restore the GBR (RRAP2023, 2023). Marine cloud brightening (MCB) is being evaluated as a potential technique to reduce the heat stress on corals (Harrison et al., 2019; Harrison, 2024). In order to assess the applicability and likely effectiveness of MCB in the GBR region it is important to understand the sources and sinks of CCN within this region. To attempt to address this question and as a part of the RRAP, the aerosol properties and the aerosol contribution to CCN were assessed in a transect voyage conducted in February and March 2022, covering parts of the central ($\sim$ 16.4 to $\sim$ 20° S) and the northern ($\sim$ 10.4 to 16.4° S) sector of the GBR.

2 Materials and methods

2.1 Survey area

Data were collected over parts of the Northern and the Central GBR from 26 February to 13 March 2022 in the Cloud-Cube container aboard the *Riverside Magnetic*, covering an area from 145 to 147° E in longitude and 14 to 19° S in latitude. The voyage track is shown below in Fig. 1. Despite its marine environment, the GBR can receive atmospheric outflows from land, carrying terrestrial and anthropogenic emissions possibly leading to greater aerosol loading and different aerosol composition (Chen et al., 2019; Fiddes et al., 2022; Hernandez-Jaramillo et al., 2024). The northern half of the Central GBR and the Northern GBR are characterised by a continuous sequence of interconnecting shelf-edge reefs, as well as massive, plentiful reefs, which are located closer to the shore than in other regions of the GBR and probably receive these outflows with increased strength and frequency (Fig. 1). Townsville and Cairns are both cities with over 500 000 inhabitants and, in addition to industry, feature a port, a marina, and an airport. Depending on the wind direction, emissions from these can thus be transported to the GBR. Air masses passing over the large areas of rainforest, particularly in Queensland's northern region, might carry an increased contribution of biogenic organic aerosols. Furthermore, regional, and long-range transport of biomass burning emissions in Northern and Eastern Australia might additionally influence the aerosol load and properties over the GBR (Mallet et al., 2017; Milic et al., 2017). In view of these potential influences to atmospheric conditions over the GBR, air mass back trajectories were generated using the Hybrid Single-Particle Lagrangian Integrated Trajectory (HYSPLIT) dispersion model (Stein et al., 2015), for all points along the ship track, to assist in attributing changes in aerosol properties to potential sources.

2.2 Cloud-Cube mobile laboratory

The Cloud-Cube (Fig. S1 in the Supplement) is a self-contained multi-instrument laboratory intended as a portable measurement station, housed in a small 8 ft shipping container with dimensions of $1700 \times 1980 \times 1835$ mm and weighing less than 1000 kg. It was designed for ease of installation on the deck of any ship, and requires limited equipment maintenance, such that it can be operated by minimal scientific staff or even the vessel crew. The container was divided into two sections: one for the instruments, which was constructed as an insulated air-conditioned chamber to keep
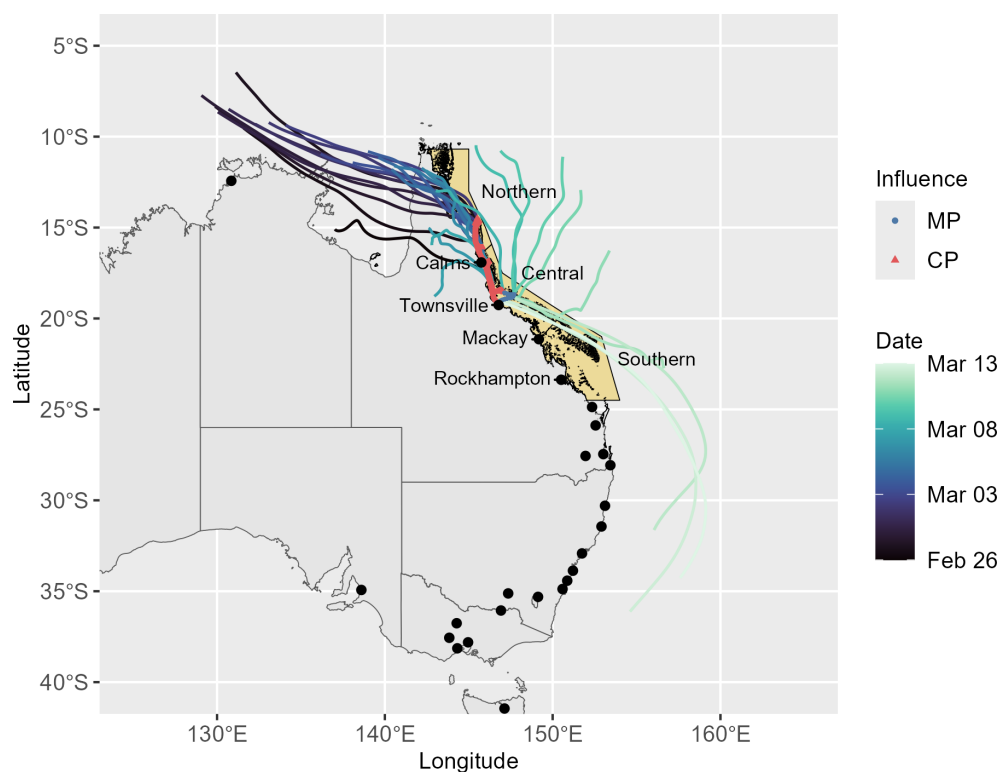
Figure 1. Voyage track for the survey in February and March 2022 aboard the *Riverside Magnetic*. The ship path is colour-coded according to whether the data shows a "continental" or "marine" influence based on the 3 d back-trajectory pathways, with continental periods (CPs) in red triangles, and marine periods (MPs) in blue points. The yellow area shows the Great Barrier Marine Park, separated into the "Northern", "Central", and "Southern" section, and the black area marks the GBR, both provided in the gisaimsr package by the Geoscience Australia (GA) and the Great Barrier Reef Marine Park Authority (GBRMPA). In addition, the 3 d air mass back trajectories at 12 h intervals (12:00 and 24:00 local time), with a trajectory starting height of 10 m above mean sea level (sampling inlet height) are presented, colour-coded by the date. The ship location marks the start point of each trajectory. The continental boundaries were obtained from the ozmaps package (https://doi.org/10.32614/CRAN.package.ozmaps, last access: 2 September 2025). Major cities were provided in the maps package (https://doi.org/10.32614/CRAN.package.maps, last access: 2 September 2025), with those with a population larger than 50 000 marked as black points and the ones along the GBR labelled.

the equipment at a moderate temperature, and another for pumps and other equipment, which had additional ventilation. A quarter of the container is sealed off from the remainder with drainage, and opens to the sky by way of a hatch in the ceiling allowing for vertically pointing instruments such as the lidar ceilometer (CL-61, Vaisala) to operate from inside the container. The container was situated in the front part of the ship. Air samples are captured through a total suspended particulate sampling inlet (URG-2000-30DG, URG) mounted on a 4 m long 3/8″ copper tube extending vertically from a corner of the Cloud-Cube container, with the inlet approximately 9 m above the ocean surface.

A particle loss calculator (von der Weiden et al., 2009) was used to estimate the size dependent particle inlet efficiency (Fig. S2), which was then utilised to correct particle size distribution observations.

The ambient relative humidity (RH) was measured by a Gill weather station (Gill MaxiMet GMX501, Gill Instruments Ltd.).

A Nafion dryer (MD700, Perma-Pure LLC) was used to dry the sample flow, and the sample line RH was monitored continuously by the Scanning Electrical Mobility Spectrometer (SEMS 2100, Brechtel Manufacturing Inc.) inbuilt sample line RH sensor.

2.3 Instrumentation

Total number concentrations of particles with diameters ≥ 7 nm was monitored using a stand-alone mixing Condensation Particle Counter (mCPC 1720, Brechtel Manufacturing Inc.).

Number size distributions of particles with diameters between 10 nm and 10 μm were measured with a Scanning Electrical Mobility Spectrometer (SEMS 2100, Brechtel Manufacturing Inc.) combined with a mCPC 1720, and an Aerodynamic Particle Sizer (APS 3321, TSI Inc.).

A Cloud Condensation Nuclei counter (CCN-100, Droplet Measurement Technologies) was provided to continuously

monitor the number of CCN and was operated in scanning mode (0.1 %, 0.2 %, 0.3 %, 0.5 %, 0.7 % supersaturation (SS) for 10 min each). Only CCN with a SS of 0.3 % were adopted in this study, if not noted otherwise, as an averaged in-cloud supersaturation of approximately 0.29 % for the continental period (CP) and 0.36 % for the marine period (MP) could be observed (classification into CPs and MPs is provided in Sect. 2.5). The Supplement includes the procedure for estimating in-cloud supersaturation. Given that the particles probably also included a mixture of other nss sulfates, organics, and a small number fraction from SSA a supersaturation of 0.3 % appears to be suitable to assess CCN properties at cloud-relevant SS levels.

Meteorological data were collected by the Gill weather station (Gill MaxiMet GMX501, Gill Instruments Ltd.).

A detailed description of the instrument configurations and the data analysis is given in the Supplement. Figure S3 depicts the sample flow arrangement for the equipment within the Cloud-Cube.

2.4 Pollution identification

The GBR is a major shipping route and is frequently influenced by anthropogenic sources from the nearby Australian coastline. As previously mentioned, continental outflow might increase the aerosol load and affect the composition of the aerosol. Periods with continental influence should not be omitted since the impact of these additional emissions on the aerosol properties are addressed in this study. To account for these regional influences while removing occasional contamination by ship exhaust from the *Riverside Magnetic*, only data within a 180° frontal arc (270 to 90°) relative to the ship's heading, and for wind speeds greater than 5 m s^{-1} were included. Short periods of rapid fluctuations and considerable increases in aerosol number concentrations were attributed to self-sampling of the ship's engine exhaust; these were removed from the data set.

2.5 Air mass categorisation and meteorological conditions

Three day back trajectories were estimated using the HYSPLIT model to identify periods that may have been influenced by continental emissions. The trajectory starting height was set to 10 m above sea level, and the meteorological data were obtained from the Global Data Assimilation System (GDAS) at a 1° spatial resolution. A more detailed description of the back-trajectory calculation is provided in Sect. S1 in the Supplement. Figure 1 shows the averaged 3 d ensemble trajectories at 12 h intervals (12:00 and 24:00 local time). Any air masses that passed over land within these 3 d prior to reaching the ship showed a clear land signature and were thus classified as CPs, all others as MPs. Continental boundaries were derived from the ArcGIS Hub (https://hub.arcgis.com/datasets/esri::

world-continents/explore?location=-0.147065%2C0. 000000%2C1.82&showTable=true, last access: 2 September 2025). However, we note that the established criteria for the CP or the MP might not adequately reflect the given conditions, such as long-range transport, local wind systems, or limitations in the accuracy of the modelled back trajectories. Thus, the distinction between marine and continental air masses is more of a qualitative guide than a guarantee of their origin.

Furthermore, locations of fire hotspots from 3 d before the sampling period in the survey area were obtained from the Sentinel Hotspots system (https://hotspots.dea.ga.gov.au/acres/sentinel, last access: 2 September 2025) using the MODIS (Moderate Resolution Imaging Spectroradiometer) sensors and VIIRS (Visible Infrared Imaging Radiometer Suite) sensors. Only hotspots with a confidence level higher than 50 % were considered in the analysis.

The temperature ranged from 23.28 to 32.38 °C over the course of the measurement period, with an average temperature of 28.09 ± 1.12 °C (median 28.28 °C). The RH ranged from 43.64 % to 90.64 %, with an average value of 75.54 ± 5.57 % (median 76.64 %). A time series of the temperature and RH for the entire period is provided in Fig. S4.

All data presented in the following have been cleaned for ship exhaust according to the method presented in Sect. 2.4

3 Results and discussion

3.1 Marine versus continental air masses

The ability of aerosols to act as CCN is affected by aerosol concentration, size distribution, and chemical composition (Andreae and Rosenfeld, 2008).

CCN number concentrations were highly variable throughout the measurement period with larger fluctuations noticed during CP, as shown in Fig. 2. The average CCN number concentration for the MP was 194 ± 72 cm^{-3} (median 196 cm^{-3}), with individual values ranging from 31 to 374 cm^{-3}. For the CP, the average was 370 ± 93 cm^{-3} (median 358 cm^{-3}), with individual values ranging from 112 to 789 cm^{-3}, which are within the range of previous observations at coastal marine sites (Schmale et al., 2018). The higher concentrations in the CP reflect that continental outflows were a contributor to CCN number concentrations in this region of the GBR.

The tendency for aerosols produced in oceanic environments to be hygroscopic enhances their ability to activate as CCN (Boucher et al., 2013). Conversely, the hygroscopicity parameter κ can be used to provide information about the aerosol composition (Petters and Kreidenweis, 2007). For example, ammonium sulfate, which has a hygroscopicity parameter κ of approximately 0.53 (Petters and Kreidenweis, 2007), is used as a surrogate for nss-sulfates. Ambient nss-sulfates are commonly internally mixed with organic species, which subsequently lower the κ value (Cravigan et al., 2020).

Zieger et al. (2017) points out a hygroscopicity parameter κ of 1.1 for inorganic sea salt. Secondary organic aerosols have a $\kappa \cong 0.1$–0.2, while biomass-burning aerosols with primarily soot particles show a κ of 0.01, and from grass burning of 0.55 (VanReken et al., 2005; Prenni et al., 2007). In organic dominated marine tropical environments with continental influence, Irwin et al. (2011) reported κ values of 0.05 to 0.37 for an SS range between 0.73 % and 0.11 %, respectively. Atwood et al. (2017) found a κ of 0.22 for a mixture of marine and biomass burning aerosols in the South China Sea/East Sea. The κ values measured in our study as shown in Fig. S5 for MP and CP at various SS levels are thus consistent with findings for marine environments with organic contribution. For all SS levels, nss-sulfates and organics tended to dominate the activated aerosol fraction, with the organic percentage being slightly larger in the CP than in the MP. This is expected given that continental outflows of both anthropogenic and biogenic origin contain a considerable amount of organic material. However, significant variations especially in continental κ were discovered, with an apparent greater number of outliers, hinting at an additional contribution of SSA to the CCN number concentrations during the CP. This in turn leads to an increase in the mean κ compared to the median κ in the CP (Fig. 2). With increasing SS, more hydrophobic aerosols such as organics activate, lowering the κ. In general, the low κ values suggest that organics contribute considerably to CCN in this region of the GBR during both the CP and the MP. No indicative difference in median κ was observed between the MP and the CP at cloud-relevant SS (Fig. 2). The κ values for the MP varied from 0.037 to 0.629, with an average of 0.188 ± 0.081 (median 0.192). For the CP, the κ values ranged from 0.006 to 1.383, with an average of 0.293 ± 0.267 (median 0.172). Sea spray enriched in organics was previously found to have low κ values and greater CCN number concentrations (Andreae and Rosenfeld, 2008; Ovadnevaite et al., 2011, 2017). This could explain our findings that the CCN number concentration in the CP is higher than in the MP, despite the somewhat lower κ.

Similar to CCN number concentrations, total particle (CN) number concentrations are higher in the CP and vary more than in the MP (Fig. 2). The average CN number concentration was $631 \pm 209 \, \text{cm}^{-3}$ (median $559 \, \text{cm}^{-3}$), with values ranging from 308 to $2468 \, \text{cm}^{-3}$ for the CP, and $387 \pm 101 \, \text{cm}^{-3}$ (median $386 \, \text{cm}^{-3}$), ranging from 139 to $728 \, \text{cm}^{-3}$ for the MP. The number concentrations in this study are thus within the range of previously reported number concentrations of approximately 400 to $800 \, \text{cm}^{-3}$ for partially continental influenced marine environments covering the same latitudinal band (Heintzenberg et al., 2000), as well as modelled total aerosol number concentrations for marine background of approximately 150 to $400 \, \text{cm}^{-3}$ (Mann et al., 2010). The fact that averaged marine concentrations are at the upper concentration range of clean marine environments further indicate a non-negligible continental contribution.

The modest changes in median κ values between the MP of 0.192 and the CP of 0.172 suggest that discrepancies in CCN number concentrations could not be attributed to differences in the hygroscopicity. The ratio between median continental CN number concentrations and median marine CN number concentrations of 1.45 is lower than the ratio between median continental CCN number concentrations and median marine CCN number concentrations of 1.83. Therefore, the differences in CCN number concentrations between the CP and the MP cannot be explained solely by the differences in CN number concentrations. As previously stated, and addressed in Andreae and Rosenfeld (2008), aerosol size distributions, which are affected by the cloud microphysical conditions in the back trajectory, are a key parameter determining the CCN number concentrations. Figure 3 presents average aerosol size distributions for MP and CP, including up to three log-normal fitted modes (dotted orange, dashed red, and dot-dashed blue) and the overall log-normal fit (solid black). The study focuses on particle sizes smaller than 500 nm due to the generally low particle number concentrations for particles larger than that.

During the MP, a bimodal particle number size distribution, where the Aitken mode (dashed red) and accumulation mode (dot-dashed blue) were separated by the Hoppel minimum, could be observed. This is consistent with cloud-processed aerosols commonly seen in marine environments (Hoppel et al., 1986; Heintzenberg et al., 2000; Seinfeld and Pandis, 2016). During the CP, an additional mode at approximately 30 nm (nucleation mode, dotted orange) was observed. Since the CP represents an average of many different continental outflow events, the Hoppel minimum is not clearly defined in the total lognormal fit (solid black line in Fig. 3). When examining the individual data points, it appears that the CP has a Hoppel minimum at 66.1 nm, which coincides with the MP minimum at 68.3 nm. The critical diameter (D_{crit}) and the Hoppel minimum for MP and CP are listed in Table S1 in the Supplement. Differences between the Hoppel minimum and D_{crit} are probably caused by the fact that the Hoppel minimum is driven by the SS during cloud processing along the back trajectory, whereas D_{crit} from the CCN is determined by the set SS during our measurements. The higher number concentrations in the CP compared to the MP mainly result from increased concentrations of particles in the accumulation mode and, to some extent, from increased concentrations in the nucleation mode. However, the latter show large standard errors, supporting the previous assumption that the air masses in this part of the GBR primarily consist of a more homogeneous background air affected by individual nucleation episodes. This can also be observed in the particle size distribution displayed in Fig. S6. The displayed averaged nucleation mode thus represents the mean of several observed nucleation events.

CCN number concentrations at cloud-relevant SS levels generally follow the particle number concentration in the accumulation mode. Due to their size, particles in this mode
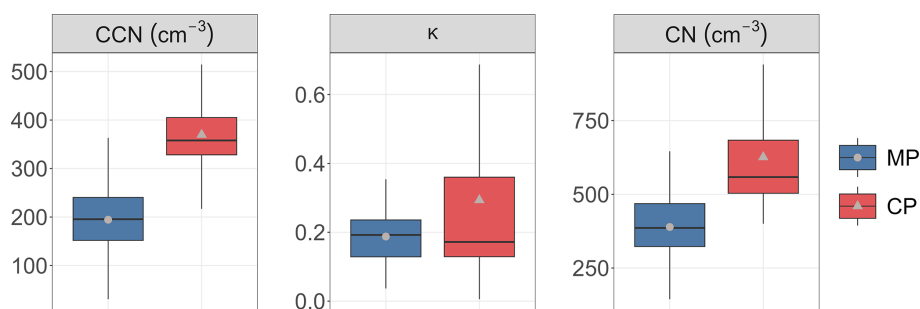
Figure 2. CCN number concentration, hygroscopicity parameter κ, and CN number concentration for the MP (blue) and the CP (red) at 0.3 % SS. The black horizontal line in a box displays the median of the individual data. The lower and upper hinges represent the 25th and 75th percentiles. The upper and lower whiskers extend from the hinge to the largest or smallest measured values, respectively, but not more than 1.5 times the difference between the 25th and 75th percentiles. The mean is shown as grey points for the MP and grey triangles for the CP.
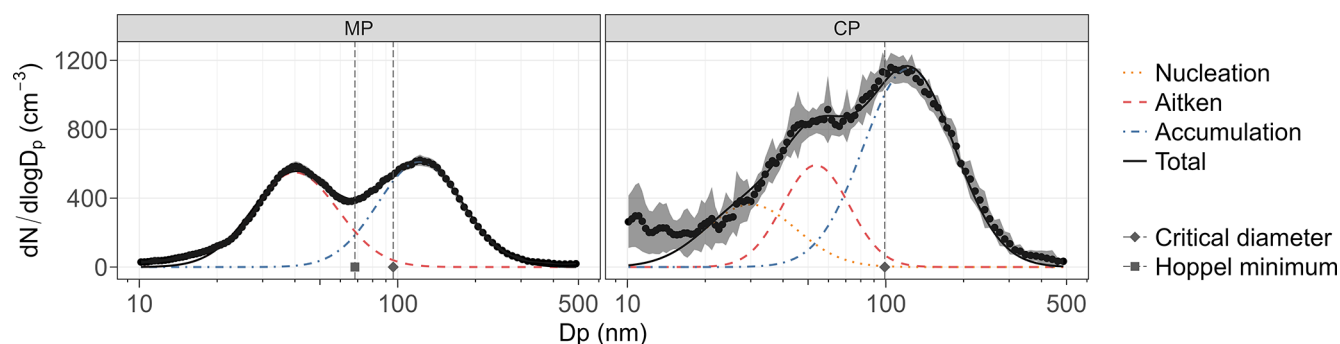
Figure 3. Average aerosol number size distributions for the MP, and the CP. The lines represent lognormal fits for an example representative nucleation mode (dotted orange), Aitken mode (dashed red), accumulation mode (dot-dashed blue), and total (solid black). The grey shaded area shows the standard deviation. The dashed grey vertical line at the diamond-shaped point represents the critical diameter (D_{crit}), whereas the dashed grey vertical line at the square-shaped point represents the Hoppel minimum.

will activate regardless of their compositions, whereas particles in the nucleation mode are expected to only play a minor role for CCN considering their small size, restricting them to activate as CCN. This could explain why the CCN number concentrations in the CP were found to be higher than those in the MP.

Cravigan et al. (2020) observed that increased organic concentrations in the ocean surface layer may result in a shift towards larger particle diameters, thus resulting in higher CCN number concentrations. Alternatively, liquid–liquid phase separation of organic-rich aerosol particles could have contributed to the enhanced CCN number concentration (Ovadnevaite et al., 2017). Both support the earlier claim that aerosol populations enriched in organic compounds can have greater CCN number concentrations despite lower κ values.

Because the displayed particle size distributions are an average and might not represent the particle size distributions of each area along the GBR, Fig. 4 shows hourly variations in the CN, and CCN number concentrations to help disentangle the impact of various sources on aerosol properties.

The CN number concentrations reveal large spikes, particularly during the CP, which could be attributed to pollution

exhaust from nearby ships, or additional continental outflows of both anthropogenic and biogenic origin. Despite these individual concentration spikes the CCN number concentration trend correlates positively with the CN number concentration. As distance from the shore increases after 7 March 2022, the CN and CCN number concentrations decrease. This suggests that individual nucleation bursts caused by increased emissions of volatile organic compounds from the dense rainforests north of Cairns or industrial emissions are better reflected in measurements collected nearshore. While bushfires are also a common source of increased number concentrations in continental outflows from northern Australia (Mallet et al., 2017; Milic et al., 2017), the Sentinel Hotspot System did not reveal any fires in the vicinity of the air mass back trajectories. Bacteria, pollen, spores, and plant debris might contribute to CCN as they are prevalent in the Aitken and accumulation modes. Secondary organic aerosol (SOA) formed through the oxidation of volatile organic compounds (VOCs) emitted by the rainforest might be an additional source of CCN, provided they have grown to a size sufficient to be CCN active. Fresh fossil fuel from diesel engines peaks in the accumulation mode, whereas petrol en-
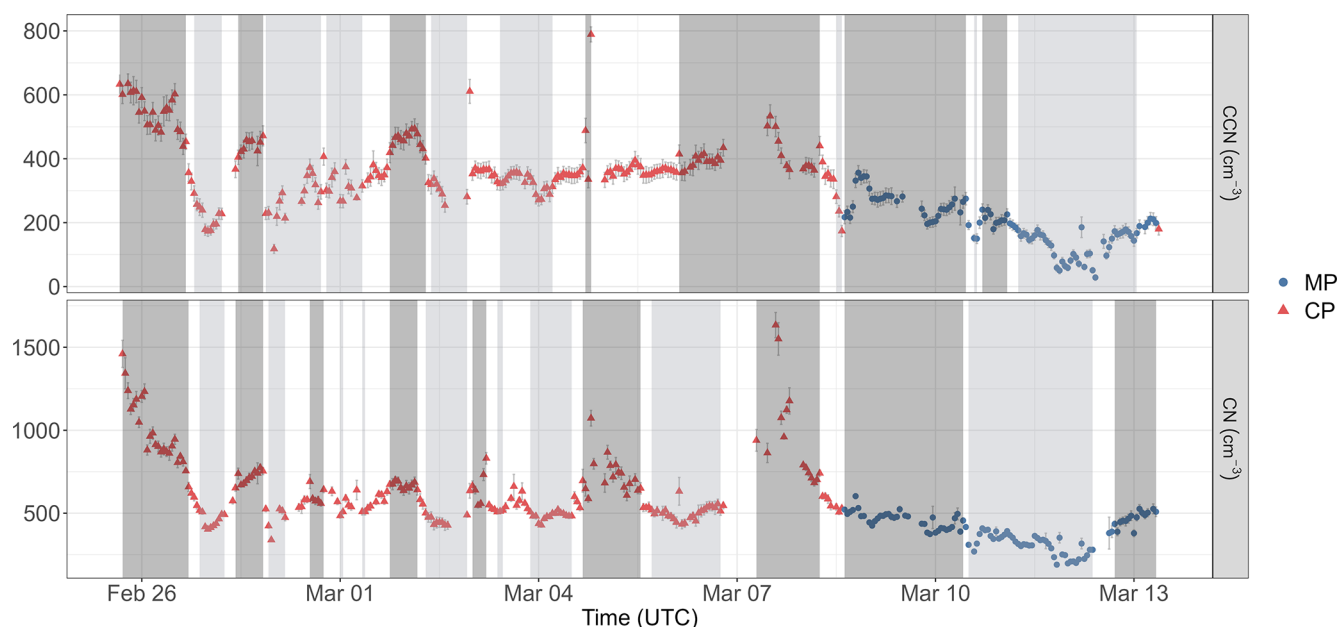
Figure 4. Hourly time series of CN, and CCN number concentrations at 0.3 % SS for the MP (blue points) and the CP (red triangles), including the standard deviation in grey. The dark-grey shaded areas represent periods with values more than 10 % above the median, whilst the light-grey shaded areas represent periods with values more than 10 % below the median.

gines exhibit smaller particle diameters predominantly in the Aitken mode. Ageing causes the particles to grow in size and become more hygroscopic, adding to CCN.

In addition to continental outflows, prior research revealed that a considerable fraction of CCN in the marine boundary layer (MBL) result from particle nucleation in the FT and/or particle entrainment from the FT into the MBL (Tunved et al., 2004; Andreae and Rosenfeld, 2008; Quinn and Bates, 2011; Clarke et al., 2013; Khadir et al., 2023). These particles are predominantly internal mixtures of organic and inorganic compounds from diverse sources (Andreae and Rosenfeld, 2008), modulated by several non-precipitation cloud processing steps and are already within a size range that is CCN active. Entrainment into the MBL occurs in the order of up to several days. Hence, for sampling locations such as the one in our study, air masses probably contain both locally formed and FT entrainment aerosol particles. Furthermore, precipitation potentially alters the CCN number concentration by lowering particle concentration in the accumulation mode (Tunved et al., 2004; Atwood et al., 2017; Khadir et al., 2023).

To determine the effects of the back-trajectory pathways, the fraction the back trajectory spent in the FT, and precipitation on CN number concentrations, aerosol size distributions, and composition, and hence eventually CCN properties, periods with a 10 % deviation from the median CN or CCN number concentrations were identified (Fig. 4). The dark-grey shaded areas reflect periods with values more than 10 % higher than the median, whereas the light-grey shaded areas represent periods with values more than 10 % lower.

The marked periods for the CN and CCN number concentrations are in good agreement, with only a few exceptions. The periods determined by the CN number concentrations will be chosen for further investigation. Each period will be discussed individually, because of the different location and air mass origin implying different aerosol sources.

3.2 High and low CN number concentration periods

Figure 5 shows the aerosol number size distributions including D_{crit} and, if present, the Hoppel minimum (top) and the 3 d back trajectories (bottom) for the seven continental high CN number concentration periods (HCP1-7). For improved visualisation, only data points every 12 h along the back trajectories are shown. Hourly resolved back trajectories are presented in Fig. S7. The aerosol size distributions and the 3 d back trajectories for the continental low CN number concentration periods (LCP1-8) are shown in Fig. S8. The Hoppel minimum and D_{crit} of all periods are additionally listed in Table S1.

The accumulation mode generally dominates in the particle size distribution. When the emission sources are located inland and mainly travelled over the Great Dividing Range in the Townsville and Cairns hinterlands (HCP1 and HCP7), the contribution to aerosols in the nucleation and Aitken modes is greater compared to when the air masses originate in the Arafura Sea. These are probably local emissions from mines, farmland, industry, and ports near the major cities along the coast. Elevated nucleation mode concentrations for air masses originating in the Arafura Sea and passing over the
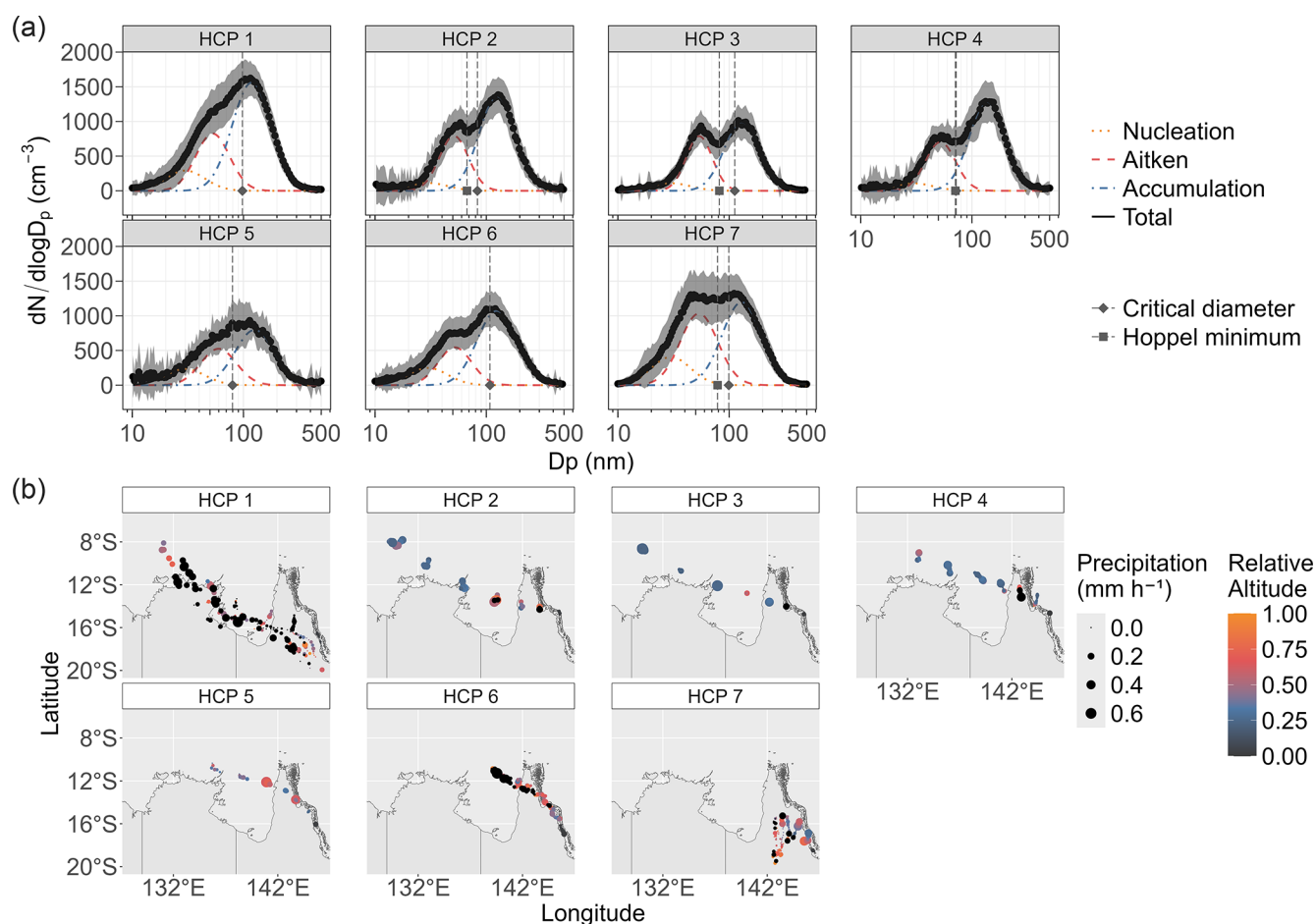
Figure 5. Average aerosol number size distributions **(a)** and the 3 d back trajectories **(b)** for the seven continental high CN number concentration periods (HCP1-7). The lines in the size distribution plots represent lognormal fits for the nucleation mode (dotted orange), Aitken mode (dashed red), accumulation mode (dot-dashed blue), and total (solid black). The dashed grey vertical line at the diamond-shaped point represents the critical diameter (D_{crit}), whereas the dashed grey vertical line at the square-shaped point represents the Hoppel minimum. Back trajectories are coloured by their altitude in respect to the planetary boundary layer height. Black data points represent air masses travelling through the FT. The precipitation amount determines the size of the trajectory points. The ship location marks the start point of each trajectory. The GBR was provided in the gisaimsr package by the GA and the GBRMPA. The continental boundaries were obtained from the ozmaps package (https://doi.org/10.32614/CRAN.package.ozmaps).

Cape York Peninsula suggest that these particles are probably SOA formed by the oxidation of VOCs emitted by the rainforest, as there are no large cities with industrial emissions in this region. However, without additional chemical composition analysis, it is impossible to clearly determine the emission source.

The Spearman correlation coefficients for a correlation significance level $p < 0.05$ between the CCN number concentration, CN number concentration inferred from the total fit, number concentration in the accumulation mode, number concentration in the Aitken mode, number concentration in the nucleation mode, averaged precipitation along one trajectory, and the percentage of time the trajectory spent in the FT for the seven continental high CN number concentration periods (HCP1-7) are displayed in Fig. S9, and for five

continental low CN number concentration periods (LCP1-2, LCP5, and LCP7-8) in Fig. S10. To align with the back-trajectory data points, the CCN number concentrations and aerosol size distributions were averaged for a period of 1 h. It should be emphasised that the Spearman correlation coefficients vary slightly based on the fit estimates for CN number concentration, and number concentrations in the accumulation and Aitken modes. Thus, the Spearman correlation coefficients shown in Figs. S9 and S10 represent only one of many possible. Nevertheless, as expected, consistently positive correlations between CCN number concentration and CN number concentration, as well as CCN number concentration and number concentration in the accumulation mode were observed, whereas no significant impact on CCN number concentration from the number concentrations in Aitken

and nucleation mode was revealed. Changes in the fraction spent in the FT, and precipitation showed a positive correlation during some events or negative during others. In general, no consistent relationship between the origin of air masses, aerosol size distribution, fraction of precipitation along the back trajectory, or time spent in the FT, and the CCN number concentration exists. This could be the case since the particle size distributions and the other metrics did not change statistically significantly during a single event. However, the two metrics that seem to have the greatest effect on the CCN number concentration in this part of the GBR during continental outflows are CN number concentration and precipitation. The marine periods present no link between the air mass origin and the particle size distribution (Figs. S11 and S12). This indicates that differences in CN and CCN number concentrations are not related to the air mass origin. Instead, it appears that the variations are caused by the air mass distance from the continent. This distance determines the relative impact of long-range transported aerosols versus local aerosol sources. The Spearman correlation coefficients (Figs. S13 and S14) again demonstrate a positive correlation between the CCN number concentration and the CN number concentration, as well as the number concentration in the accumulation mode. In addition, a positive correlation in the Aitken mode was noticed. Precipitation exhibited a consistent negative influence. Compared to the continental periods, where CCN number concentration affecting factors vary greatly from period to period, marine periods provide a more consistent picture given that marine aerosol populations are more homogeneous in size and composition than continental aerosol populations. Nonetheless, a larger dataset would be necessary to adequately evaluate correlations between various parameters.

3.3 CCN activation ratio

To further understand the impact of CCN number concentrations on cloud formation, CCN activation ratios (CCN / CN) were calculated. CCN / CN is determined by D_{crit} for CCN activation, which is inversely associated with κ. D_{crit} is shown by vertical lines in the size distributions in Figs. 5, S7, S8, S11, and S12 and values are listed in Table S1. Figure S15 presents the CCN / CN ratios for MP and CP at various SS levels. For all SS levels, the activated aerosol fraction, is larger in the CP than in the MP. However, separating the CCN / CN at the cloud-relevant SS level into the distinct periods demonstrates that the situation is not straightforward (Figs. 6 and S16). In general, there is no clear correlation between the air mass pathways and origin and their CCN / CN ratios.

4 Conclusion and outlook

In situ atmospheric data sets were obtained in February and March 2022 to characterise aerosol sources, aerosol size dis-

tributions, and CCN properties in the Central and Northern GBR. These measurements have the ability to improve our understanding on aerosol-cloud interactions in this region.

The CCN concentrations were highly variable during the voyage, with average CCN number concentration for the MP of $194 \pm 72\,\mathrm{cm^{-3}}$ (median $196\,\mathrm{cm^{-3}}$), and $370 \pm 93\,\mathrm{cm^{-3}}$ (median $358\,\mathrm{cm^{-3}}$) for the CP. The higher concentrations in the CP suggest a considerable influence from continental emissions to CCN number concentrations in this region of the GBR.

The hygroscopicity parameter κ suggests an internally mixed composition of nss-sulfates and organics for both the MP and CP, with a higher organic contribution during the CP compared to the MP. Given that continental outflows of both anthropogenic and biogenic origin contain a considerable amount of organic material this is not surprising. In general, the low κ values suggest that organics contribute considerably to CCN in this region of the GBR during both the CP and the MP. The averaged κ values for the MP were 0.188 ± 0.081 (median 0.192), and for the CP 0.293 ± 0.267 (median 0.172). No indicative difference in median κ was observed between the MP and the CP at cloud-relevant SS. Low κ values and greater CCN number concentrations for sea spray enriched in organics were previously observed by Andreae and Rosenfeld (2008), Ovadnevaite et al. (2011), and Ovadnevaite et al. (2017). This could explain that in our study the CCN number concentration in the CP is higher than in the MP, despite the somewhat lower κ.

The average CN number concentration for the CP was $631 \pm 209\,\mathrm{cm^{-3}}$ (median $559\,\mathrm{cm^{-3}}$), and $387 \pm 101\,\mathrm{cm^{-3}}$ (median $386\,\mathrm{cm^{-3}}$) for the MP. A distinct bimodal aerosol number size distribution, with a clear Aitken and accumulation mode, separated by the Hoppel minimum, as expected for cloud-processed marine aerosols were observed during MP. Higher CN number concentrations in the accumulation mode were assumed to be the reason for the higher CCN number concentrations in the CP compared to the MP.

However, the Spearman correlation coefficients for a correlation significance level $p < 0.05$ between the CCN number concentration, CN number concentration inferred from the total fit, number concentration in the accumulation mode, number concentration in the Aitken mode, number concentration in the nucleation mode, averaged precipitation along one trajectory, and the percentage of time the trajectory spent in the FT reveal that no consistent relationship between the origin of air masses, size distribution, fraction of precipitation along the back trajectory, or time spent in the FT, and the CCN number concentration exists. The two metrics that seem to have the greatest effect on the CCN number concentration in this part of the GBR during continental outflows are CN number concentration and precipitation along the back-trajectory pathway. Future measurements would benefit from co-located measurements of particle number size distributions, CCN number concentrations, and precipitation rates to better understand the impact of local precipitation. Marine
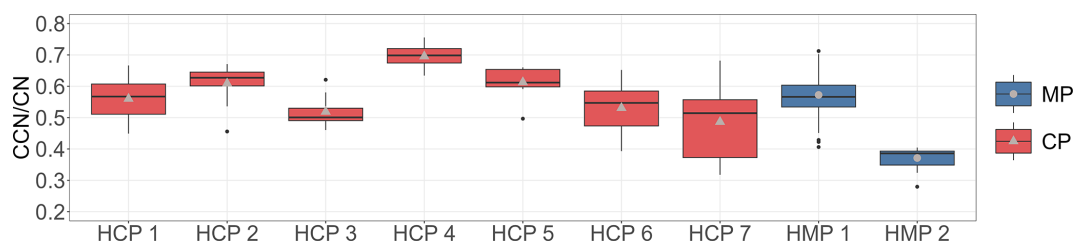
Figure 6. CCN activation ratios (CCN / CN) at 0.3 % SS for the MP (blue) and the CP (red) for the high CN number concentration periods (HCP1-7 and HMP1-2). The black horizontal line in a box displays the median of the individual data. The lower and upper hinges represent the 25th and 75th percentiles. The upper and lower whiskers extend from the hinge to the largest or smallest measured values, respectively, but not more than 1.5 times the difference between the 25th and 75th percentiles. The mean is shown as grey points for the MP and grey triangles for the CP. Outliers are individual data points that fall outside of this range and are colour-coded black.

periods also indicate a positive correlation with the number concentration in the Aitken and accumulation mode.

The activated aerosol fraction is larger in the CP than in the MP. However, the CCN / CN for the distinct periods are similar in some of the continental and marine periods, and there is no apparent association between air mass paths and origins and their CCN / CN ratios.

The Cooling and Shading subprogram within the RRAP is investigating the feasibility of two independent technologies, MCB and fogging, to minimise the amount of solar radiation reaching the GBR. The data will help to identify sections of the GBR that would benefit the most from MCB. Due to energy and economic constraints, it may be desirable to limit MCB implementation to sub-regions of the GBR. Locations that would be best suited for implementing MCB on the GBR are determined not only by where it is most needed, but also by where it will be most effective. Therefore, to target the optimum increase in cloud albedo from activation of the aerosol into cloud droplets, the background aerosol properties need to be known. The implications for MCB are that if we know the typical number concentration of aerosols in the marine background that can act as CCN and how these vary across the GBR, we can estimate how many cloud seeding particles of a known size need to be injected to increase the cloud droplet number concentration and achieve the required cloud brightening. To achieve a climatological understanding of aerosol and CCN properties over the GBR long-term continuous measurements will be required to capture the variety of atmospheric conditions more comprehensively over the entire latitudinal range of the sparsely observed GBR. This includes both transect voyages as well as stationary observations spanning several bleaching seasons. The results presented here represent a first step over the northern segment of the GBR for which no previous data exist.

Author contributions. EJH analysed the data and prepared the manuscript. JA conducted the instrument installation and analysed the data. LH conducted the instrument installation and remote monitoring throughout the voyage and designed the Cloud-Cube. LC conducted the instrument installation. DPH conceived the project, obtained funding, supervised the project and conceived and designed the Cloud-Cube. ZDR supervised the project.

References

Andreae, M. O. and Rosenfeld, D.: Aerosol–cloud–precipitation interactions. Part 1. The nature and sources of cloud-active aerosols, Earth Sci. Rev., 89, 13–41, https://doi.org/10.1016/j.earscirev.2008.03.001, 2008.

ArcGIS Data and Maps Esri - World Continents, ArcGIS Hub [data set], https://hub.arcgis.com/datasets/esri::world-continents/explore?location=-0.147065%2C0.000000%2C1.82&showTable=true, 2024.

Atwood, S. A., Reid, J. S., Kreidenweis, S. M., Blake, D. R., Jonsson, H. H., Lagrosas, N. D., Xian, P., Reid, E. A., Sessions, W. R., and Simpas, J. B.: Size-resolved aerosol and cloud condensation nuclei (CCN) properties in the remote marine South China Sea – Part 1: Observations and source classification, Atmos. Chem. Phys., 17, 1105–1123, https://doi.org/10.5194/acp-17-1105-2017, 2017.

Barneche, D., and Murray, L.: Assortment of GBR GIS Files, GitHub [data set], https://github.com/open-aims/gisaimsr/, 2020.

Becker, R. A, Wilks, A. R., Brownrigg, R., Minka, T. P., and Deckmyn, A.: maps: Draw Geographical Maps, CRAN [code], https://doi.org/10.32614/CRAN.package.maps, 2025.

Berkelmans, R., De'ath, G., Kininmonth, S., and Skirving, W. J.: A comparison of the 1998 and 2002 coral bleaching events on the Great Barrier Reef: Spatial correlation, patterns and predictions, Coral Reefs, 23, 74–83, https://doi.org/10.1007/s00338-003-0353-y, 2004.

Boucher, O., Randall, D., Artaxo, P., Bretherton, C., Feingold, G., Forster, P., Kerminen, V.-M., Kondo, Y., Liao, H., Lohmann, U., Rasch, P., Satheesh, S. K., Sherwood, S., Stevens, B., and Zhang, X. Y.: Clouds and Aerosols, in: Climate Change 2013: The Physical Science Basis. Contribution of Working Group I to the Fifth Assessment Report of the Intergovernmental Panel on Climate Change (IPCC), Cambridge University Press, Cambridge, 571–657, ISBN 978-92-9169-138-8, 2013.

Chen, Z., Schofield, R., Rayner, P., Zhang, T., Liu, C., Vincent, C., Fiddes, S., Ryan, R. G., Alroe, J., Ristovski, Z. D., Humphries, R. S., Keywood, M. D., Ward, J., Paton-Walsh, C., Naylor, T., and Shu, X.: Characterization of aerosols over the Great Barrier Reef: The influence of transported continental sources, Sci. Total Environ., 690, 426–437, https://doi.org/10.1016/j.scitotenv.2019.07.007, 2019.

Clarke, A. D., Freitag, S., Simpson, R. M. C., Hudson, J. G., Howell, S. G., Brekhovskikh, V. L., Campos, T., Kapustin, V. N., and Zhou, J.: Free troposphere as a major source of CCN for the equatorial pacific boundary layer: long-range transport and teleconnections, Atmos. Chem. Phys., 13, 7511–7529, https://doi.org/10.5194/acp-13-7511-2013, 2013.

Condie, S. A., Anthony, K. R., Babcock, R. C., Baird, M. E., Beeden, R., Fletcher, C. S., Gorton, R., Harrison, D., Hobday, A. J., Plagányi, É. E., and Westcott, D. A.: Large-scale interventions may delay decline of the Great Barrier Reef, Roy. Soc. Open Sci., 8, 201296, https://doi.org/10.1098/rsos.201296, 2021.

Cravigan, L. T., Mallet, M. D., Vaattovaara, P., Harvey, M. J., Law, C. S., Modini, R. L., Russell, L. M., Stelcer, E., Cohen, D. D., Olsen, G., Safi, K., Burrell, T. J., and Ristovski, Z.: Sea spray aerosol organic enrichment, water uptake and surface tension effects, Atmos. Chem. Phys., 20, 7955–7977, https://doi.org/10.5194/acp-20-7955-2020, 2020.

Cropp, R., Gabric, A., van Tran, D., Jones, G., Swan, H., and Butler, H.: Coral reef aerosol emissions in response to irradiance stress in the Great Barrier Reef, Australia, Ambio, 47, 671–681, https://doi.org/10.1007/s13280-018-1018-y, 2018.

Fiddes, S. L., Woodhouse, M. T., Lane, T. P., and Schofield, R.: Coral-reef-derived dimethyl sulfide and the climatic impact of the loss of coral reefs, Atmos. Chem. Phys., 21, 5883–5903, https://doi.org/10.5194/acp-21-5883-2021, 2021.

Fiddes, S. L., Woodhouse, M. T., Utembe, S., Schofield, R., Alexander, S. P., Alroe, J., Chambers, S. D., Chen, Z., Cravigan, L., Dunne, E., Humphries, R. S., Johnson, G., Keywood, M. D., Lane, T. P., Miljevic, B., Omori, Y., Protat, A., Ristovski, Z., Selleck, P., Swan, H. B., Tanimoto, H., Ward, J. P., and Williams, A. G.: The contribution of coral-reef-derived dimethyl sulfide to aerosol burden over the Great Barrier Reef: a modelling study, Atmos. Chem. Phys., 22, 2419–2445, https://doi.org/10.5194/acp-22-2419-2022, 2022.

GBRMP: Great Barrier Reef Marine Park, Australian Institute of Marine Science, and CSIRO 2023, Reef snapshot: Summer 2022-23, Great Barrier Reef Marine Park Authority, Townsville, ISBN 978-0-6450438-6-0, 2023.

Harrison, D. P., Baird, M., Harrison, L., Utembe, S., Schofield, R., Escobar Correa, R., Mongin, M., and Rizwi, F.: Reef Restoration and Adaptation Program: Environmental Modelling of Large-Scale Solar Radiation Management. A report provided to the Australian Government by the Reef Restoration and Adaptation Program, 83 pp., https://gbrrestoration.org/wp-content/uploads/2020/09/T14-Environmental-Modelling-of-Large-Scale-SRM_v3.03-3.pdf (last access: 2 September 2025), 2019.

Harrison, D. P.: An overview of environmental engineering methods for reducing coral bleaching stress, in: Oceanographic Processes of Coral Reefs, edited by: Wolanski, E. and Kingsford, M. J., CRC Press, Boca Raton, Florida, USA, 403–418, https://doi.org/10.1201/9781003320425, 2024.

Heintzenberg, J., Covert, D., and Van Dingenen, R.: Size distribution and chemical composition of marine aerosols: a compilation and review, Tellus B, 52, 1104–1122, https://doi.org/10.3402/tellusb.v52i4.17090, 2000.

Hernandez-Jaramillo, D. C., Medcraft, C., Braga, R. C., Butcherine, P., Doss, A., Kelaher, B., Rosenfeld, D., and Harrison, D. P.: New airborne research facility observes sensitivity of cumulus cloud microphysical properties to aerosol regime over the great barrier reef, Environ. Sci.: Atmos., 4, 861–871, https://doi.org/10.1039/d4ea00009a, 2024.

Hock, K., Doropoulos, C., Gorton, R., Condie, S. A., and Mumby, P. J.: Split spawning increases robustness of coral larval supply and inter-reef connectivity, Nat. commun., 10, 3463, https://doi.org/10.1038/s41467-019-11367-7, 2019.

Hoppel, W. A., Frick, G. M., and Larson, R. E.: Effect of non-precipitating clouds on the aerosol size distribution in the marine boundary layer, Geophys. Res. Lett., 13, 125–128, https://doi.org/10.1029/GL013i002p00125, 1986.

Horchler, E. J., Alroe, J., Harrison, L., Cravigan, L., Harrison, D., and Ristovski, Z.: Aerosol and cloud nuclei properties along the Central and Northern Great Barrier Reef: Impact of continental emissions, Version v1, Zenodo [data set], https://doi.org/10.5281/zenodo.15064303, 2025.

Hughes, T. P., Kerry, J. T., Álvarez-Noriega, M., Álvarez-Romero, J. G., Anderson, K. D., Baird, A. H., Babcock, R. C., Beger, M.,

Bellwood, D. R., Berkelmans, R., Bridge, T. C., Butler, I. R., Byrne, M., Cantin, N. E., Comeau, S., Connolly, S. R., Cumming, G. S., Dalton, S. J., Diaz-Pulido, G., Eakin, C. M., Figueira, W. F., Gilmour, J. P., Harrison, H. B., Heron, S. F., Hoey, A. S., Hobbs, J. A., Hoogenboom, M. O., Kennedy, E. V., Kuo, C. Y., Lough, J. M., Lowe, R. J., Liu, G., McCulloch, M. T., Malcolm, H. A., McWilliam, M. J., Pandolfi, J. M., Pears, R. J., Pratchett, M. S., Schoepf, V., Simpson, T., Skirving, W. J., Sommer, B., Torda, G., Wachenfeld, D. R., Willis, B. L., and Wilson, S. K.: Global warming and recurrent mass bleaching of corals, Nature, 543, 373–377, https://doi.org/10.1038/nature21707, 2017.

Irwin, M., Robinson, N., Allan, J. D., Coe, H., and McFiggans, G.: Size-resolved aerosol water uptake and cloud condensation nuclei measurements as measured above a Southeast Asian rainforest during OP3, Atmos. Chem. Phys., 11, 11157–11174, https://doi.org/10.5194/acp-11-11157-2011, 2011.

Jackson, R., Gabric, A., and Cropp, R.: Effects of ocean warming and coral bleaching on aerosol emissions in the Great Barrier Reef, Australia, Sci. Rep., 8, 14048, https://doi.org/10.1038/s41598-018-32470-7, 2018.

Khadir, T., Riipinen, I., Talvinen, S., Heslin-Rees, D., Pöhlker, C., Rizzo, L., Machado, L. A. T., Franco, M. A., Kremper, L. A., Artaxo, P., Petäjä, T., Kulmala, M., Tunved, P., Ekman, A. M. L., Krejci, R., and Virtanen, A.: Sink, source or something in-between? Net effects of precipitation on aerosol particle populations, Geophys. Res. Lett., 50, e2023GL104325, https://doi.org/10.1029/2023GL104325, 2023.

Leahy, S. M., Kingsford, M. J., and Steinberg, C. R.: Do clouds save the Great Barrier Reef? Satellite imagery elucidates the cloud-SST relationship at the local scale, PLoS One, 8, e70400, https://doi.org/10.1371/journal.pone.0070400, 2013.

Mallet, M., Cravigan, L., Miljevic, B., Vaattovaara, P., Deschaseaux, E., Swan, H., Jones, G., and Ristovski, Z.: Sea spray aerosol in the Great Barrier Reef and the presence of non-volatile organics, J. Geophys. Res.-Atmos., 121, 7088–7099, https://doi.org/10.1002/2016JD024966, 2016.

Mallet, M. D., Desservettaz, M. J., Miljevic, B., Milic, A., Ristovski, Z. D., Alroe, J., Cravigan, L. T., Jayaratne, E. R., Paton-Walsh, C., Griffith, D. W. T., Wilson, S. R., Kettlewell, G., van der Schoot, M. V., Selleck, P., Reisen, F., Lawson, S. J., Ward, J., Harnwell, J., Cheng, M., Gillett, R. W., Molloy, S. B., Howard, D., Nelson, P. F., Morrison, A. L., Edwards, G. C., Williams, A. G., Chambers, S. D., Werczynski, S., Williams, L. R., Winton, V. H. L., Atkinson, B., Wang, X., and Keywood, M. D.: Biomass burning emissions in north Australia during the early dry season: an overview of the 2014 SAFIRED campaign, Atmos. Chem. Phys., 17, 13681–13697, https://doi.org/10.5194/acp-17-13681-2017, 2017.

Mann, G. W., Carslaw, K. S., Spracklen, D. V., Ridley, D. A., Manktelow, P. T., Chipperfield, M. P., Pickering, S. J., and Johnson, C. E.: Description and evaluation of GLOMAP-mode: a modal global aerosol microphysics model for the UKCA composition-climate model, Geosci. Model Dev., 3, 519–551, https://doi.org/10.5194/gmd-3-519-2010, 2010.

Masson-Delmotte, V., Zhai, P., Pirani, A., Connors, S. L., Péan, C., Berger, S., Caud, N., Chen, Y., Goldfarb, L., Gomis, M. I., Huang, M., Leitzell, K., Lonnoy, E., Matthews, J., Maycock, T. K., Waterfield, T., Yelekçi, O., Yu, R., and Zhou, B. (Eds.): IPCC 2021: Summary for Policymakers, in: Climate Change 2021: The Physical Science Basis. Contribution of Working Group I to the Sixth Assessment Report of the Intergovernmental Panel on Climate Change, Cambridge University Press, Cambridge, United Kingdom and New York, NY, USA, https://doi.org/10.1017/9781009157896, 2021.

Milic, A., Mallet, M. D., Cravigan, L. T., Alroe, J., Ristovski, Z. D., Selleck, P., Lawson, S. J., Ward, J., Desservettaz, M. J., Paton-Walsh, C., Williams, L. R., Keywood, M. D., and Miljevic, B.: Biomass burning and biogenic aerosols in northern Australia during the SAFIRED campaign, Atmos. Chem. Phys., 17, 3945–3961, https://doi.org/10.5194/acp-17-3945-2017, 2017.

Murphy, D. M., Anderson, J. R., Quinn, P. K., McInnes, L. M., Brechtel, F. J., Kreidenweis, S. M., Middlebrook, A. M., Pósfai, M., Thomson, D. S., and Buseck, P. R.: Influence of sea-salt on aerosol radiative properties in the Southern Ocean marine boundary layer, Nature, 392, 62–65, https://doi.org/10.1038/32138, 1998.

Ovadnevaite, J., Ceburnis, D., Martucci, G., Bialek, J., Monahan, C., Rinaldi, M., Facchini, M. C., Berresheim, H., Worsnop, D. R., and O'Dowd, C.: Primary marine organic aerosol: A dichotomy of low hygroscopicity and high CCN activity, Geophys. Res. Lett., 38, L21806, https://doi.org/10.1029/2011GL048869, 2011.

Ovadnevaite, J., Zuend, A., Laaksonen, A., Sanchez, K. J., Roberts, G., Ceburnis, D., Decesari, S., Rinaldi, M., Hodas, N., Facchini, M. C., Seinfeld, J. H., and O'Dowd, C.: Surface tension prevails over solute effect in organic-influenced cloud droplet activation, Nature, 546, 637–641, https://doi.org/10.1038/nature22806, 2017.

Petters, M. D. and Kreidenweis, S. M.: A single parameter representation of hygroscopic growth and cloud condensation nucleus activity, Atmos. Chem. Phys., 7, 1961–1971, https://doi.org/10.5194/acp-7-1961-2007, 2007.

Prenni, A. J., Petters, M. D., Kreidenweis, S. M., DeMott, P. J., and Ziemann, P. J.: Cloud droplet activation of secondary organic aerosol, J. Geophys. Res., 112, D10223, https://doi.org/10.1029/2006JD007963, 2007.

Quinn, P. K., and Bates, T. S.: The case against climate regulation via oceanic phytoplankton sulphur emissions, Nature, 480, 51–56, https://doi.org/10.1038/nature10580, 2011.

Quinn, P. K., Coffman, D. J., Johnson, J. E., Upchurch, L. M., and Bates, T. S.: Small fraction of marine cloud condensation nuclei made up of sea spray aerosol, Nat. Geosci., 10, 674–679, https://doi.org/10.1038/ngeo3003, 2017.

RRAP2023: https://gbrrestoration.org/, last access: 8 November 2023.

Seinfeld, J. H. and Pandis, S. N.: Atmospheric Chemistry and Physics: From Air Pollution to Climate Change, 3rd edn., John Wiley & Sons, Inc., New York, 719–720, ISBN 9781119221166, 2016.

Schmale, J., Henning, S., Decesari, S., Henzing, B., Keskinen, H., Sellegri, K., Ovadnevaite, J., Pöhlker, M. L., Brito, J., Bougiatioti, A., Kristensson, A., Kalivitis, N., Stavroulas, I., Carbone, S., Jefferson, A., Park, M., Schlag, P., Iwamoto, Y., Aalto, P., Äijälä, M., Bukowiecki, N., Ehn, M., Frank, G., Fröhlich, R., Frumau, A., Herrmann, E., Herrmann, H., Holzinger, R., Kos, G., Kulmala, M., Mihalopoulos, N., Nenes, A., O'Dowd, C., Petäjä, T., Picard, D., Pöhlker, C., Pöschl, U., Poulain, L., Prévôt, A. S. H., Swietlicki, E., Andreae, M. O., Artaxo, P., Wiedensohler, A., Ogren, J., Matsuki, A., Yum, S. S., Stratmann, F.,

Baltensperger, U., and Gysel, M.: Long-term cloud condensation nuclei number concentration, particle number size distribution and chemical composition measurements at regionally representative observatories, Atmos. Chem. Phys., 18, 2853–2881, https://doi.org/10.5194/acp-18-2853-2018, 2018.

Stein, A. F., Draxler, R. R., Rolph, G. D., Stunder, B. J., Cohen, M. D., and Ngan, F.: NOAA's HYSPLIT Atmospheric Transport and Dispersion Modeling System, B. Am. Meteorol. Soc., 96, 2059–2077, https://doi.org/10.1175/bams-d-14-00110.1, 2015.

Stuart-Smith, R. D., Brown, C. J., Ceccarelli, D. M., and Edgar, G. J.: Ecosystem restructuring along the Great Barrier Reef following mass coral bleaching, Nature, 560, 92–96, https://doi.org/10.1038/s41586-018-0359-9, 2018.

Sumner, M., Cook, D., Herenu, D.: ozmaps: Australia Maps, CRAN [code], https://doi.org/10.32614/CRAN.package.ozmaps, 2021.

Tunved, P., Ström, J., and Hansson, H.-C.: An investigation of processes controlling the evolution of the boundary layer aerosol size distribution properties at the Swedish background station Aspvreten, Atmos. Chem. Phys., 4, 2581–2592, https://doi.org/10.5194/acp-4-2581-2004, 2004.

VanReken, T. M., Ng, N. L., Flagan, R. C., and Seinfeld, J. H.: Cloud condensation nucleus activation properties of biogenic secondary organic aerosol, J. Geophys. Res., 110, D07206, https://doi.org/10.1029/2004JD005465, 2005.

von der Weiden, S.-L., Drewnick, F., and Borrmann, S.: Particle Loss Calculator – a new software tool for the assessment of the performance of aerosol inlet systems, Atmos. Meas. Tech., 2, 479–494, https://doi.org/10.5194/amt-2-479-2009, 2009.

Zhao, W., Huang, Y., Siems, S., and Manton, M.: The role of clouds in coral bleaching events over the Great Barrier Reef, Geophys. Res. Lett., 48, e2021GL093936, https://doi.org/10.1029/2021GL093936, 2021.

Zhao, W., Huang, Y., Siems, S., and Manton, M.: A characterization of clouds over the Great Barrier Reef and the role of local forcing, Int. J. Climatol., 42, 6647–6664, https://doi.org/10.1002/joc.7660, 2022.

Zhao, W., Huang, Y., Siems, S., Manton, M., and Harrison, D.: Interactions between trade wind clouds and local forcings over the Great Barrier Reef: a case study using convection-permitting simulations, Atmos. Chem. Phys., 24, 5713–5736, https://doi.org/10.5194/acp-24-5713-2024, 2024.

Zieger, P., Väisänen, O., Corbin, J. C., Partridge, D. G., Bastelberger, S., Mousavi-Fard, M., Rosati, B., Gysel, M., Krieger, U. K., Leck, C., Nenes, A., Riipinen, I., Virtanen, A., and Salter, M. E.: Revising the hygroscopicity of inorganic sea salt particles, Nat. Commun., 8, 15883, https://doi.org/10.1038/ncomms15883, 2017.